Available online at www.sciencedirect.com
SCIENCE DIRECT
Nuclear Instruments and Methods in Physics Research A 562 (2006) 371–379
NUCLEAR INSTRUMENTS & METHODS IN PHYSICS RESEARCH Section A
www.elsevier.com/locate/nima

Studies on the response of ^{3}He and ^{4}He proportional counters to monoenergetic fast neutrons

M. Manolopoulou[a,*], M. Fragopoulou[a], S. Stoulos[a], C. Koukorava[a], A. Spyrou[b], G. Perdikakis[b], S.R. Hashemi-Nezhad[c], M. Zamani[a]

[a]*School of Physics, Aristotle University of Thessaloniki, Thessaloniki 54124, Hellas, Greece*
[b]*NCSR Democritos, Athens, Hellas, Greece*
[c]*School of Physics, A28, University of Sydney, NSW 2006, Australia*

Received 1 September 2005; received in revised form 7 January 2006; accepted 5 February 2006
Available online 9 March 2006

Abstract

Two helium filled proportional counters (^{3}He and ^{4}He) were studied to establish the optimum operating conditions when these counters are used for fast neutron measurements, as well as to examine the linearity of the pulse height with neutron energy. The detectors were irradiated with mono-energetic neutrons in the energy range of 230 keV–22 MeV, produced via ^{7}Li(n,p)^{7}Be, ^{2}H(d,n)^{3}He and ^{3}H(d,n)^{4}He reactions in a Tandem Van de Graff accelerator. The gamma ray contribution to the obtained pulse height distribution and the resolution of the counters as a function of shaping time constant and applied high voltage were studied.

PACS: 29.30.Hs; 29.40.Cs

Keywords: ^{3}He; ^{4}He; Proportional counters; Neutron detectors; Neutron measurements

1. Introduction

Helium filled proportional counters are widely used in the field of neutron detection and spectrometry [1,2]. ^{3}He counter is used mainly in measurements of thermal-epithermal neutrons. It can be used for fast neutron measurements, but its efficiency is limited. ^{4}He detector is suitable for measurement of fast neutrons; above 1 MeV [2]. The different response of the two helium counters is attributed to the different interaction cross-sections of neutrons with ^{3}He and ^{4}He in various energy regions (Fig. 1). In the case of the ^{3}He detectors both ^{3}He(n,p)^{3}H reactions and ^{3}He(n,elastic) contribute to the pulse height distribution while in ^{4}He counters ^{4}He(n,elastic) is the main contributor to the observed pulses. In thermal-epithermal region ^{3}He(n,p)^{3}H reaction is predominant, while at neutron energies $E_n \sim 1$ MeV the ^{4}He(n,elastic) cross-section is about four times higher than that of the ^{3}He(n,elastic) [3].

As already mentioned, the ^{3}He counter is usually utilized for thermal-epithermal neutron measurements. For the correct estimation of the number of thermal neutrons, the contribution of other sources (gamma rays, recoils, etc.) to the thermal peak as well as their influence on to the resolution of this peak needs to be known. Furthermore, this type of counter could also be used, with reasonable efficiency, up to 2 MeV. In this work the general characteristics of two commercially available counters, a ^{3}He and a ^{4}He, were studied in order to specify the optimal operating conditions when they are used for measuring neutrons with energies up to several MeV. The energy calibration of the detectors was performed by irradiation with mono-energetic neutron beams in the energy region from 230 keV to 22 MeV using the Tandem, Van de Graff accelerator facility at the Institute of Nuclear Physics, NCSR Demokritos, Athens, Hellas. The influence of the shaping time constant on the pulse height distribution and to the behavior of the gamma ray component, which

*Corresponding author. Tel./fax: +30 2310998217.
E-mail address: metaxia@auth.gr (M. Manolopoulou).

0168-9002/$ - see front matter © 2006 Elsevier B.V. All rights reserved.
doi:10.1016/j.nima.2006.02.040

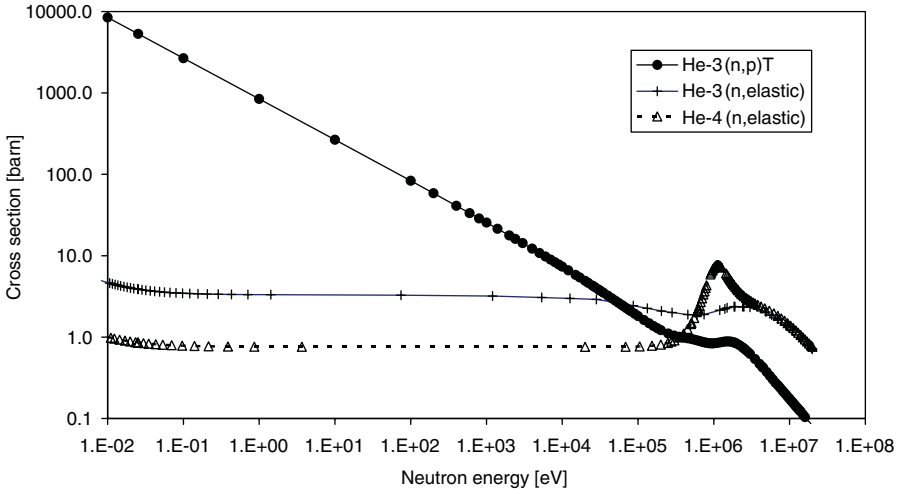

Fig. 1. Cross-sections of ^{3}He and ^{4}He reactions with neutrons, as a function of neutron energy [3].

contributes to the low end of the pulse height distribution, was studied. Finally, the resolution of the detectors as a function of neutron energy and applied high voltage was determined.

2. Experimental

The basic characteristics of the two commercially available cylindrical proportional counters[1] used in this study are summarized in Table 1. The measurement system consists of a high voltage power supply, a preamplifier suitable for proportional counters (Canberra model 2006), an amplifier (Tennelec model TC243 or Canberra model 2025) and a computer-based multichannel analyzer (Tennelec PCA III or Canberra model Multiport II).

Neutrons with energies E_n, in the range of 230 keV–3.3 MeV were obtained via ^{7}Li(p,n)^{7}Be reaction. When the projectile energy is above 2.2 MeV, besides the neutrons from ^{7}Li(p,n)^{7}Be reaction with ^{7}Be at ground state (n_0 neutrons) a second group of neutrons are also emitted from ^{7}Li(p,n)^{7}Be* reaction (n_1 neutrons, 0.429 MeV) [4]. At projectile energies above 3.68 MeV neutrons from ^{7}Li(p, n ^{3}He)^{4}He reaction and at energies above 7.06 MeV neutrons from ^{7}Li(p, n)^{7}Be reaction (n_2 neutrons, with excitation of the second excited state of ^{7}Be) start contributing to the overall neutron yield. Among these, the n_1 neutrons have the highest yield and at energies below 5 MeV, used in this study, the zero-degree yield of these low energy neutrons is less than 10% of the n_0 neutrons [5].

The peak due to neutrons from ^{7}Li(p,n)^{7}Be* reaction is clearly distinguishable from the peak of the main neutron group (Fig. 2), due to the energy difference between the neutrons emitted from these two reactions as well as due to the relatively smaller cross-section of the second reaction [6]. Thus, the second neutron group does not affect the measurements on the characteristic peak values of the main neutron group. As an example, in Fig. 2 the two peaks corresponding to 2019 keV (due to ^{7}Li(p,n)^{7}Be) and 1561 keV (due to ^{7}Li(p,n)^{7}Be*) are marked with arrows. The reason for attributing these peaks to n_1 neutrons and not to wall effect is that, in all pulse height distributions shown in Fig. 2, the energies of the small peaks appearing prior to the main peaks, are equal (within experimental errors) to those expected for n_1 neutrons. Due to the large diameter of the ^{3}He detector used (5 cm), its high pressure (6 atm) and high Kr content the probability of wall effect is significantly less than the cases one can observe in a smaller detector with lower pressure of the gas content.

Neutron energies in the range of 3.75–10.7 MeV were produced from ^{2}H(d,n)^{3}He reaction. The mean energy loss of the projectile energy in the target gas cell (Mo, 5.1 mg cm^{-2}) was calculated using the SRIM/TRIM code [7]. When the deuteron energy is above 4.45 MeV its break-up produces a neutron continuum. As a result, the mono-energetic range of the above reaction extends up to neutron energy of 7.7 MeV, produced at projectile energies $\leqslant$4.45 MeV. The maximum energy of neutron continuum (resulting from the deuteron break-up) has an energy difference of $\sim$7 MeV for neutrons parallel to the primary reaction neutrons [8]. Therefore, this neutron continuum does not interfere with the peak of the primary neutrons. Larger neutron energies, up to 22 MeV, were obtained via ^{3}H(d,n)^{4}He reaction.

The detectors were positioned with the anode wire parallel to the projectile beam direction at 0°. Due to the geometrical arrangement of the detectors with respect to the projectile beam direction and because of the size of openings of the detectors, neutrons with energies other than the 0° neutron energy can also enter the detector volume (Fig. 3). In each of the irradiations the deviations from the 0° neutron energy and mean energies of these neutrons were calculated by weighting the neutron energies with their intensities at relevant directions. Angular

[1] ^{3}He was manufactured by LND Inc., New York, USA and ^{4}He by Eurisys Mesures, France.

Table 1
Characteristics of the counters

	Pressure (atm)	Gas content (%)	Cathode material/ thickness (cm)	Anode material/ diameter (mm)	Effective length (cm)	Effective diameter (cm)
^{3}He	6	^{3}He 64.7 Kr 33.3 CO_2 2.0	Stainless steel 304/ 0.089	Tungsten/0.025	15	5
^{4}He	18	^{4}He 99.2 CO_2 0.8	Stainless steel 304/ 0.125	Tungsten/0.050	60	5

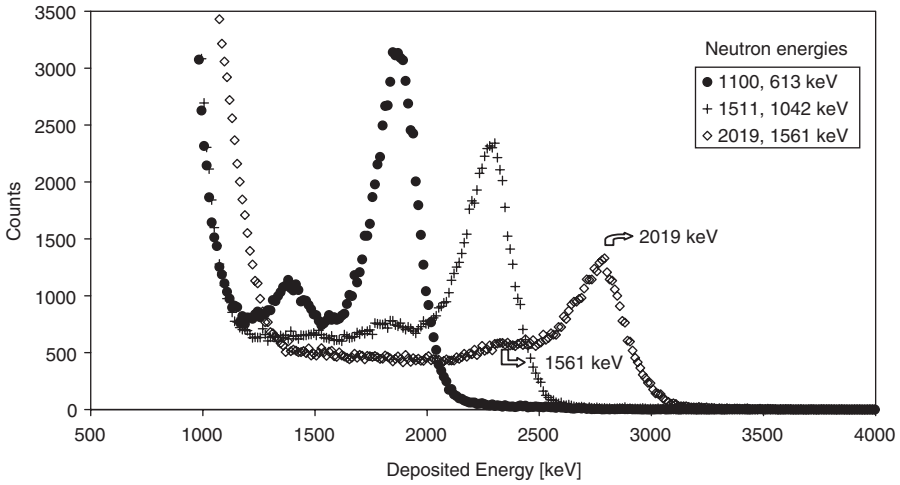

Fig. 2. Some of pulse height distributions obtained with ^{3}He counter. The two group of neutron energies that are emitted from ^{7}Li(p,n)^{7}Be and ^{7}Li(p,n)^{7}Be* reactions are clearly distinguishable in each distribution.

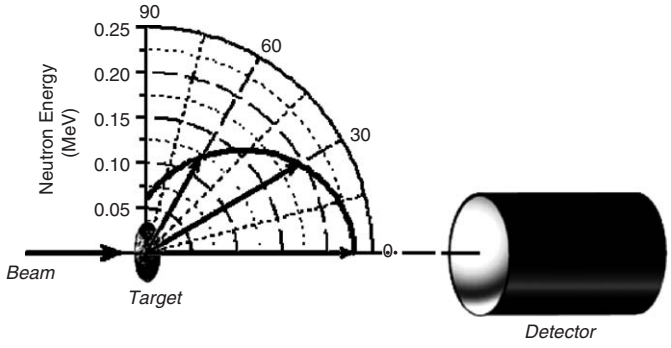

Fig. 3. Arrangement of the detectors with respect to the beam direction. As an example neutron energy as a function of the emission angle is presented for the case of ^{7}Li(p,n)^{7}Be reaction when proton energy is 2 MeV.

dependences of laboratory cross-sections and energies were calculated using the DROSG-2000 code [6]. The calculated difference between mean neutron energies and the energies of neutrons at 0° varied from 0.1% to 0.3%.

The detectors were also irradiated with gamma rays from a ^{137}Cs source (100 μCi) and with a collimated electron beam from a ^{90}Sr–^{90}Y source (5 mCi), in order to determine the appropriate shaping time constant (τ) for neutron–gamma discrimination. The τ varied from 2 to 12 μs.

3. Results and discussion

3.1. Analysis of pulse height distributions

In gas proportional counters both neutrons and gamma rays give rise to detected pulses. Typical pulse height distributions collected with ^{4}He and ^{3}He counters are presented in Fig. 4a and b, respectively. In ^{4}He counter the major part of registered pulses originate from the recoiled ^{4}He nuclei due to ^{4}He(n,elastic) reaction. In the absence of other phenomena, such as partially deposited energy due to the wall effect or electronic effects, the expected shape of the pulse height distribution has the same shape as differential cross-section, $d\sigma(E_n)/d\Omega$, of the ^{4}He(n,elastic) reaction [9]. The pulse height distributions obtained with ^{4}He detector (Fig. 4a) are composed of:

(1) A peak due to the recoiled ^{4}He nuclei with recoil angle $\theta_{lab} = 0°$, when all of their energy is deposited within the sensitive volume of the detector. These nuclei produce the peaks appearing in Fig. 4a. The maximum energy, E_{max}, transferred to the recoiling ^{4}He nucleus

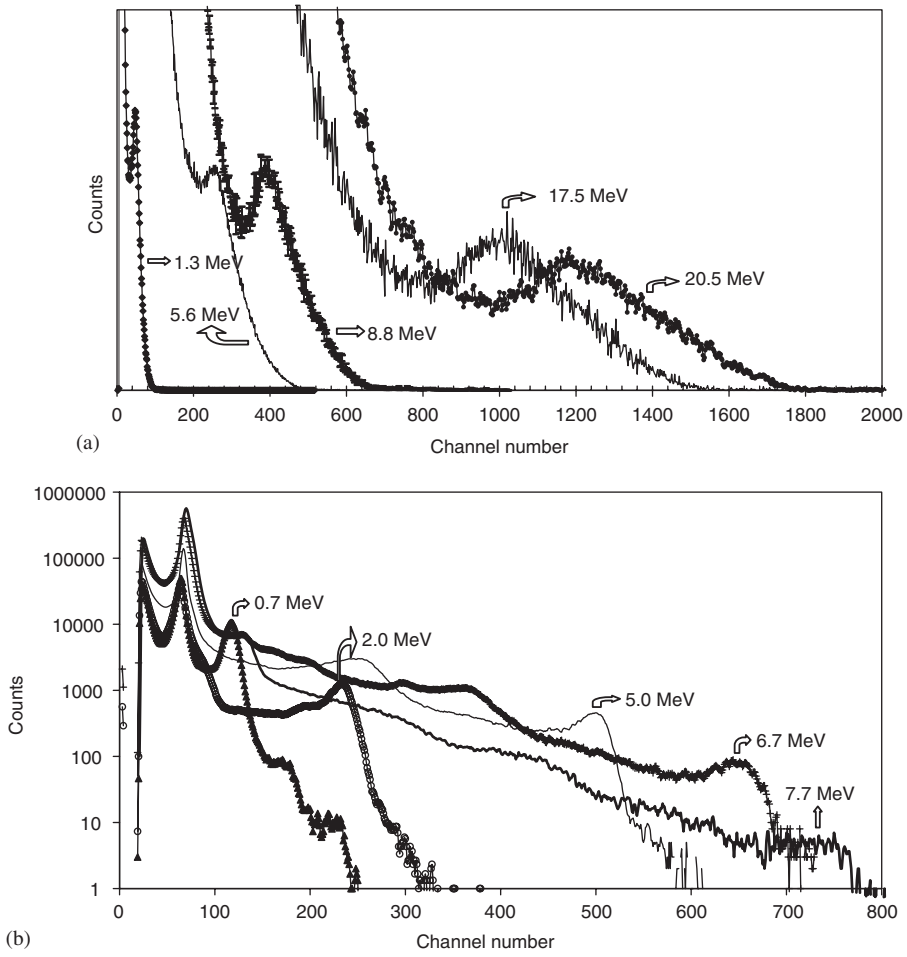

Fig. 4. (a) Pulse height distributions obtained with ^{4}He counter when the detector was irradiated with neutrons of different energies. The abscissa units are different for each distribution. (b) Pulse height distributions obtained with ^{3}He when the detector was irradiated with neutrons of different energies.

traveling in the direction of the incoming neutron, is $E_n*(4mM)/(m+M)^2 = 0.64*E_n$ where E_n is neutron energy, M and m are the masses of ^{4}He and neutron, respectively. A fitting procedure was applied to these peaks in order to calculate the centroid channel and the FWHM value.

(2) ^{4}He recoil nuclei that deposit part of their energies within the detector volume and the rest in the detector wall (the wall effect). These recoils can have a continuum of all possible energies up to E_{max}.

(3) Recoil nuclei of the other gases (C,O) present in the detector volume.

In the case of the ^{3}He detector as well as all the above-mentioned processes (i.e. pulses due to the recoils of the nuclei present in the detector gas: ^{3}He, Kr, C, O) a peak due to the ^{3}He(n,p)^{3}H reaction can also be seen (which will be referred to as the full energy peak) . As the Q value of this reaction is 764 keV, the total kinetic energy of the reaction products is $E_n + 764$ keV. A peak due to this energy is formed when both of the reaction products (i.e. p and ^{3}H) deposit all their energies within the detector volume. This peak appears towards the higher end of the pulse height distributions shown in Fig. 4b. As the maximum proton energy which can be totally absorbed in our ^{3}He counter is about 7 MeV, the probability of registering pulses at full-energy peak decreases rapidly for neutrons above this energy because of increased probability of the wall effects (Fig. 4b). Finally, at neutron energies above 4.4 MeV the ^{3}He(n,d)^{2}H reaction starts to take place. As the Q value of this reaction is -3.27 MeV, the total kinetic energy of the reaction products produce a peak in the pulse height distributions at energy E_n-3.27 MeV.

In a way similar to the ^{4}He recoils, the ^{3}He recoils have a maximum energy of $0.75*E_n$. The maximum energy of the recoil of other nuclei in the gas mixture is significantly less, that is $0.05*E_n$ for Kr, $0.29*E_n$ for C and $0.22*E_n$ for O. Finally, in all pulse height distributions of the ^{3}He counter a peak is observed at 764 keV which is due to the thermal-epithermal neutrons. These low energy neutrons result from neutron scattering by material present in the irradiation hall (e.g. floor, walls, etc.).

3.2. Irradiations with gamma and beta rays

Gamma rays interacting mainly with the counter wall produce small pulses which are registered in the low energy end of the pulse height distributions. Helium nuclei scattered at wide angles as well as the recoil nuclei of the other gases present in the detectors, also contributes to this part of the distributions. The gamma ray contribution to the pulse height distribution of ^{3}He counter can extend almost up to the thermal neutron peak [10]. Under normal operating conditions neutrons and gamma rays are effectively distinguished from each other by rise time discrimination, since, typically, pulses originating from gamma rays have longer rise times [9]. Spectra collected using gamma and beta rays show similar behavior in both detectors. They contribute to the low energy end of the pulse height distribution with the count number exponentially decreasing as channel number increases. Data collected with various shaping time constants were very well fitted ($R^2 > 99.95\%$) with the function

$$\text{Counts} = a\,\mathrm{e}^{-b\ \text{channel}}. \quad (1)$$

In Figs. 5a and b the variation of b in Eq. (1) as a function of shaping time constant τ, are presented for ^{3}He and ^{4}He detectors, respectively. The two data sets in each figure correspond to cases when the detectors were irradiated with a collimated electron beam (^{90}Sr/^{90}Y source) in directions perpendicular and parallel to the anode wire. The same figures show the corresponding dead time of ADC. There is a sharp decrease of b values as the shaping time increases from 2 to 4 μs, indicating that the majority of gamma and beta rays produce pulses with rise times approximately of this value. As expected, the dead time increases proportionally with τ, due to the increase in the processing time of the pulses and also because, of the number of pulses with height greater than the lower level discriminator of the ADC (which was set at 100 mV).

The difference in the dead time observed between the two detectors should be partially attributed to the different fraction of the electron beam absorbed in the detector wall due to the variation of the wall thickness (Table 1). For example, from electron range calculation (csda) in stainless steel it is deduced that electrons with energy lower than 1.1 and 1.5 MeV for ^{3}He and ^{4}He counters, respectively, are totally absorbed in the detector wall. Hence the fraction of ^{90}Y beta decay spectrum (maximum energy 2.28 MeV) that would penetrate the detectors cover would be 38% and 17%, respectively.

Another important factor which can increase the response of ^{3}He detector is the higher probability of photons produced by ionization–excitation processes by electrons, which have passed through the metal cover, to interact with the gas mixture in the ^{3}He detector with its high Kr ($Z = 36$) content. The absolute dead time in both detectors is smaller when the beta ray source is placed on the base of the detector (parallel irradiation). In this case a fraction of the electrons and/or electrons kinetic energy is absorbed in the dead layer of the gas as they pass through it, before entering the effective volume of the detector. For example, electrons with residual kinetic energy (after penetrating the base) less than 60–70 keV would be totally absorbed in this layer (csda). In addition, photons produced on the cylindrical side of the counter (perpendicular irradiation) have about 1.5 times larger probability of interaction with the gas or the metal cover than the ones produced on the base due to the different geometry factor. Finally, the dead time growth rate, or equivalently the count rate growth, in case of the irradiation performed perpendicularly to the ^{3}He detector axis, is much more rapid, indicating that in this case there is relatively larger number of smaller pulses than in the case of the parallel irradiation, in accordance with the above justification.

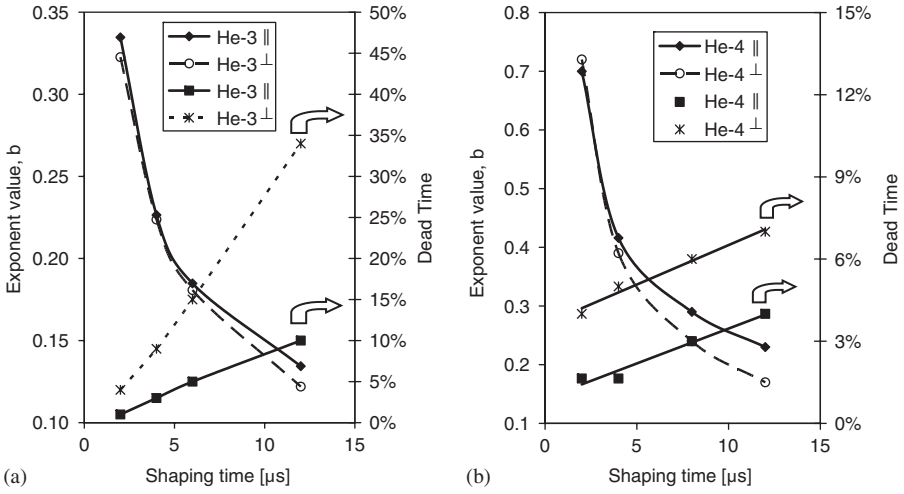

Fig. 5. Variation of the dead time and exponent value, b, of the function: counts $= a.\mathrm{e}^{-b\,\text{channel}}$ for (a) ^{3}He and (b) ^{4}He counters as a function of shaping time. Detectors were irradiated with electrons in direction parallel ∥ and perpendicular ⊥ to the anode wire.

3.3. Irradiations with neutron beams

The influence of τ on the pulse height distributions obtained with ^{4}He counter for neutron beam energies of 4.4 and 10.7 MeV is presented in Figs. 6a and b, respectively. A ballistic deficit was observed with the variation of the shaping time. Significant loss of resolution with small shaping time settings is statistically significant only in higher energies.

The energy resolution of the ^{3}He counter for thermal-epithermal neutrons as a function of high voltage and shaping time constant is presented in Fig. 7a. These measurements were performed by exposing the detector to thermal neutrons from a ^{241}Am–Be source, covered with paraffin moderator. In Fig. 7a higher values of FWHM with decreasing high voltage settings should be attributed to statistical fluctuations in the gas amplification, recombination and electronic noise, effects that broaden the peak in a Gaussian mode. Higher resolution values are observed when high voltage increases due to an enhanced asymmetry in the peak shape. The same phenomenon, observed by Dietz et al. [1], was ascribed to space charge effect since, they found a correlation, although weak, of the asymmetry of the peak with a larger number of preamplifier pulses having long rise times. Due to the negligible momentum of thermal-epithermal neutrons the reaction products, proton and triton, are emitted in opposite directions. Longer rise times are attributed to those cases where the proton and the triton travel almost perpendicularly to the anode wire, with maximum of the ionization near the end of their track.

In order to clarify if the reason for increasing peak asymmetry is the same in our case, we did some measurements using thermal neutrons. Rise times of the preamplifier pulses and the amplitudes of the corresponding amplifier pulses were measured at two HV settings using a Tektronix oscilloscope (model TDS3052B). Only those pulses belonging to the thermal peak (764 keV) were counted. The amplifier gain was adjusted in such a way that the right-hand side of the thermal peaks coincide in the two HV settings. We measured 1000 pulses at each HV setting. The measurements for each HV setting were grouped in two parts, according to their amplitude with respect to their centroid amplitude. The results, presented in Table 2, show that enhanced asymmetry of the peak (higher HV) is correlated to larger number of longer rise time pulses.

The observed difference in the mean rise time between the lower and higher amplitude pulses can be qualitatively explained by the self-induced space charge effect. The avalanches created by the first primary electrons arriving in the multiplication region prevent the avalanche growth of the subsequent primary electrons, when the proton and triton trajectories are almost perpendicular to the anode. As HV increases the electron density in the avalanche region becomes higher and thus enhancing this phenomenon and resulting in lower amplitude pulses and increasing peak asymmetry. When the trajectories are almost parallel to anode wire the primary electron density is less, resulting in a larger avalanche size [11]. These cases correspond to the larger amplitude pulses.

The difference in the pulse rise time of the preamplifier is more obvious in the ^{3}He detector used in this study probably because of the Kr content, in which the electron drift velocity is low. Other factors that enhance such self-induced space charge effect are those that result in higher primary electron density along the anode; such as the geometry of the tube and the magnitude of the gas multiplication [9].

The energy resolution of ^{4}He recoil peaks as a function of HV for neutron energies of 5.6 and 6.7 MeV are presented in Fig. 7b.The relatively large values of resolution for ^{4}He counter should be partially attributed to the

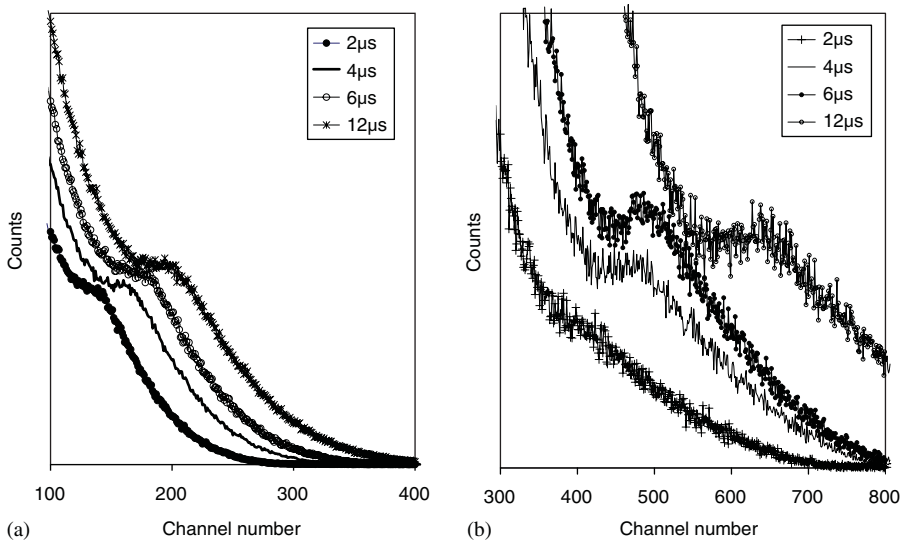

Fig. 6. Pulse height distributions obtained using ^{4}He counter with different shaping time constants τ, for neutron energies of (a) 4.4 MeV and (b) 10.7 MeV. The abscissa units are different for each distribution.

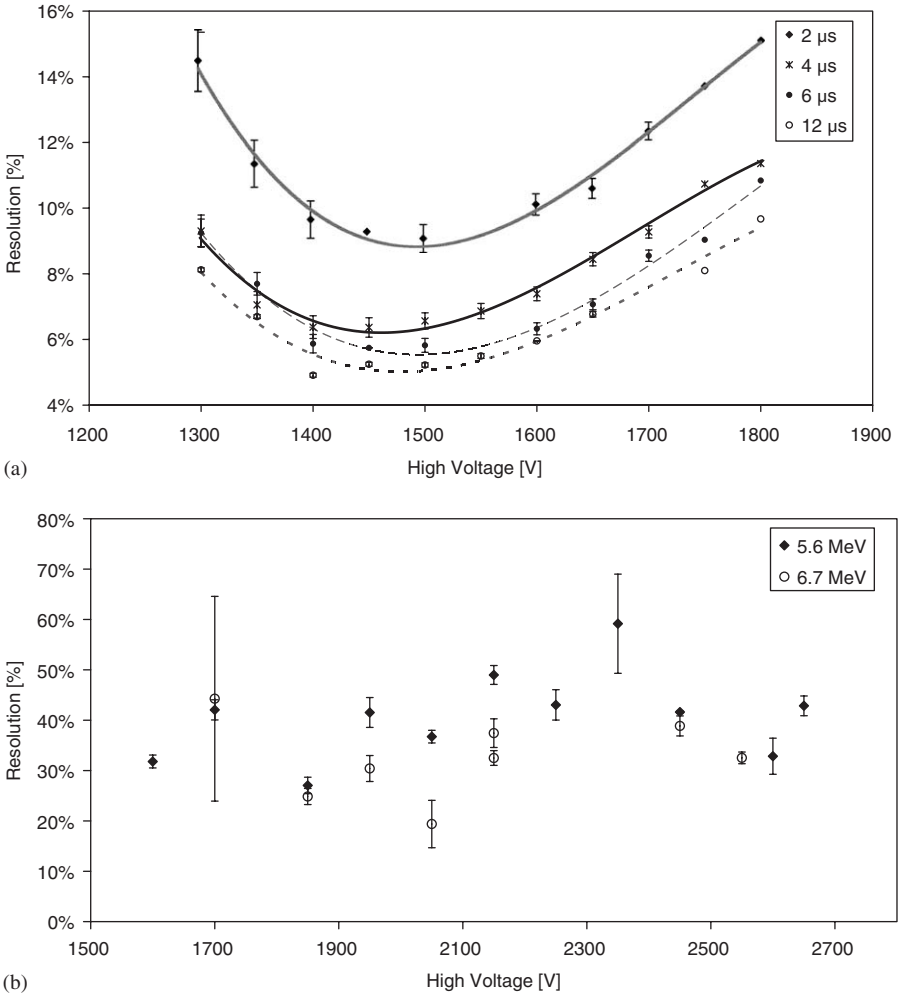

Fig. 7. (a) The energy resolution of ^{3}He counter at 764 keV, as a function of high voltage and shaping time constant. The lines are third-order polynomial fittings to guide the eye. (b) The energy resolution of the ^{4}He-recoil peaks in ^{4}He counter as a function of high voltage for two neutron energies of 5.6 and 6.7 MeV. The measurements were performed with shaping time constant of 6 μs.

Table 2
The variation of mean rise time of preamplifier pulses for 764 keV peak (thermal neutrons) grouped according to the amplitude of the corresponding amplifier pulses, in two HV settings

High voltage	Pulses with amplitude less than that of the centroid	Pulses with amplitude greater than that of the centroid
1760 V		
Mean rise time ($\pm 1\sigma$) (μs)	2.23($\pm$0.46)	1.93($\pm$0.33)
Percentage of pulses counted in each group	53.9	46.1
Confidence intervals for difference of means 99% (μs)	Lower limit: 0.22	Upper limit: 0.37
1640 V		
Mean rise time $\pm 1\sigma$ (μs)	2.09($\pm$0.50)	1.91($\pm$0.59)
Percentage of pulses counted in each group	50.2	49.8
Confidence intervals for difference of means 99% (μs)	Lower limit: 0.06	Upper limit: 0.28

origin of the recoil peak, as this is not mono-energetic due to $d\sigma(E_n)/d\Omega$ distribution. There is, however, no statistically significant variation of the resolution of the counter with the applied high voltage. For both detectors the measurements were carried out in the proportionality region.

From the above findings it seems that, although a shaping time constant of 2 μs would be more appropriate for neutron–gamma discrimination, larger values are needed in order to avoid deterioration in resolution and departure from linearity, when neutron energies up to several MeV are being measured. Thus, for both counters

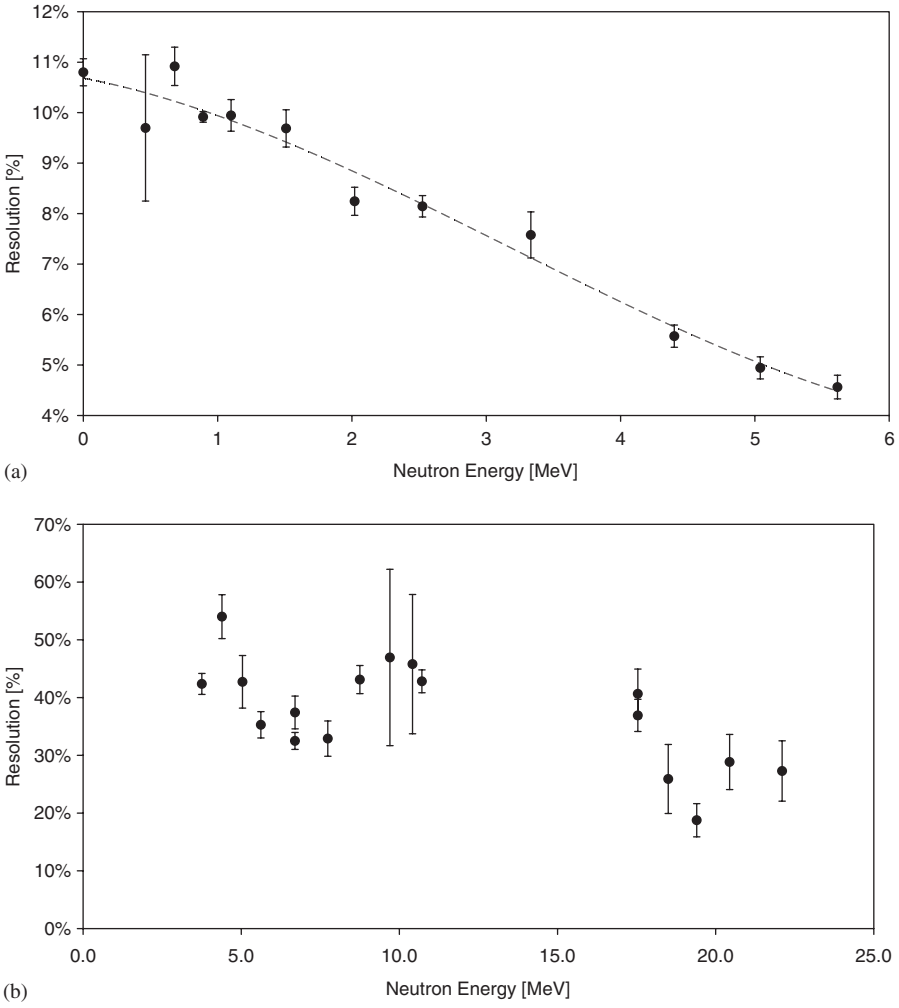

Fig. 8. (a) ^{3}He counter resolution as a function of neutron energy, at HV = 1650 V. The resolution was calculated for the full energy peak. The line is a polynomial fitting of third order. (b) ^{4}He counter resolution as a function of neutron energy, at HV = 2150 V.

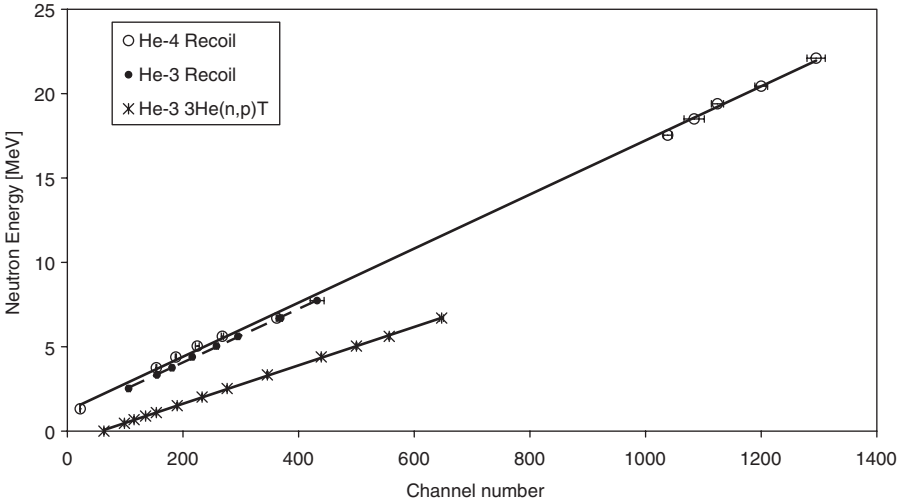

Fig. 9. Energy calibration of ^{3}He and ^{4}He counters, as a function of incident neutron energy. The irradiations were performed parallel to anode wire. The shaping time constant was 6 μs for both detectors and HV supply was 2150 and 1650 V for ^{4}He and ^{3}He counters, respectively.

the shaping time constant of 6 μs was selected as a compromise between the resolution loss and dead time increment (Fig. 5).

The energy resolution of the two counters as a function of neutron energy is presented in Fig. 8. As expected, the resolution of ^{3}He counter clearly decreases with neutron energy. Although the resolution of ^{4}He counter seems to follow a similar trend, significant conclusion cannot be drawn because of the relatively high statistical uncertainty.

The energy calibration of the detectors was performed with the neutron beam parallel to the anode wire. For all peaks (i.e. ^{3}He and ^{4}He recoils and ^{3}He(n,p)^{3}H) a linear response with the neutron energy was observed (Fig. 9).

4. Summary

The operational characteristics of ^{3}He and ^{4}He counters were studied for neutron energies up to 22 MeV. Gamma ray contribution to the pulse height distributions for both counters exhibited an exponential behavior with irradiations both perpendicularly and parallel to anode wire. A higher response of the ^{3}He detector to beta and gamma rays is attributed mainly to a smaller cathode thickness and to relatively high Kr content in the gas mixture. Gamma ray contribution can be minimized with small shaping time constant settings. On the contrary, a larger shaping time constant is needed to improve the resolution of both counters. In view of this the shaping time constant for this study was set at 6 μs.

A linear response with incident neutron energy was observed for both detectors in the energy range studied, with the incident irradiation beam parallel to the anode wire. The ^{3}He counter studied in this work can be used for neutron spectroscopy up to 7 MeV. The centroid of the peak formed by the ^{4}He nuclei recoiling in neutron beam direction, has a linear dependency on neutron energy up to 22 MeV.

For ^{3}He detectors the resolution for the thermal-epithermal neutron peak deteriorates at large high voltage settings, a behavior attributable to the effect of self-induced space charge. At neutron energies up to 7 MeV the resolution of ^{3}He counter was in the range of 4–11% for the full-energy peak. The resolution for ^{4}He recoil peaks in the ^{4}He counter varied from 52% to 22% for the neutron energy in the range of 4–22 MeV.

Acknowledgments

The authors would like to thank the operating staff of Tandem accelerator, NCSR, Demokritos, for providing the neutron beams and technical support. Especially we would like to thank N. Divis, N. Papakostopoulos and V. Andreadis for their continuous interest and technical help.

References

[1] E. Dietz, M. Matzke, W. Sosaat, G. Urbach, M. Weyrauch, Nucl. Instr. and Meth. A 332 (1993) 521.
[2] M. Weyrauch, A. Casnati, P. Schillebeeckx, M. Clapham, Nucl. Instr. and Meth. A 403 (1998) 442.
[3] ENDF/B-VI evaluated nuclear data file. Database Version of February 24, 2005. www.nndc.bnl.gov/exfor/endf00.htm
[4] C.A. Uttley, Neutron Physics and Nuclear data in Science and Technology, vol. 2, Neutron Sources for Basic Physics and Applications, An OECD/NEA Report, Pergamon, 1983.
[5] S.G. Mashnik, M.B. Chadwick, H.G. Hughes, R.C. Little, R.E. MacFarlane, L.S. Waters, P.G. Young, Los Alamos National Laboratory, September 1, 2005, available at: http://arxiv.org/list/nucl-th/0011066
[6] DROSG-2000: Neutron Source Reactions, Data files with computer codes for 57 accelerator-based neutron source reactions. Version 2.2 (January 2003) prepared by M. Drosg, Institute for Experimental Physics, University of Vienna, Austria. Available at: http://www-nds.iaea.org/drosg2000.html.
[7] J.F. Ziegler, J.P. Biersack, U. Littmark, Stopping and Ranges of Ions in Matter, Pergamon Press, New York, 1985 (see also: SRIM/TRIM The Stopping and Range of Ions in Matter. www.srim.org).
[8] M. Drosg, O. Schwerer, Handbook on Nuclear Activation Data, Technical Report Series No. 273, IAEA, Vienna, 1987.
[9] G.F. Knoll, Radiation Detection and Measurement, third ed, Wiley, New York, 1999.
[10] D.H. Beddingfield, N.H. Johnson, H.O. Menlove, Nucl. Instr. and Meth. A 455 (2000) 670.
[11] T. Horiguchi, T. Itoh, T. Yamamoto, T. Miyasaka, J. Sakai, K. Shibata, Y. Masuda, A. Okumura, T. Niwa, Nucl. Instr. and Meth. A 529 (2004) 369.